Mean and maximum two dimensional wind force on an open-grown tree

Angelou, Nikolas; Gardiner, Barry; Dellwik, Ebba

Published in:
Journal of Wind Engineering and Industrial Aerodynamics

Link to article, DOI:
10.1016/j.jweia.2024.105966

Publication date:
2025

Document Version
Publisher's PDF, also known as Version of record

Journal of Wind Engineering & Industrial Aerodynamics 257 (2025) 105966

Contents lists available at ScienceDirect

Journal of Wind Engineering & Industrial Aerodynamics

journal homepage: www.elsevier.com/locate/jweia

Mean and maximum two dimensional wind force on an open-grown tree

Nikolas Angelou [a,*], Barry Gardiner [b,c], Ebba Dellwik [a]

[a] Department of Wind Energy, Technical University of Dermark (DTU), Frederiksborgvej 399, 4000 Roskilde, Denmark
[b] Institut Européen de la Forêt Cultivée, Cestas, France
[c] Chair of Forestry Economics and Forest Planning, Albert-Ludwigs-University Freiburg, Freiburg, Germany

ARTICLE INFO

Keywords:
Open-grown trees
Wind load
Wind force
Wind-tree interaction
Extreme wind load
Strain gauge transducer

ABSTRACT

The accurate quantification of the wind loading on trees is crucial for estimating the risk of tree damage. Here, we present an experimental quantification of the wind force on a rural, open-grown, deciduous tree. We first demonstrate that the amplitude and direction of the two-dimensional force vector can be estimated using two strain gauges mounted on the bottom of the stem. Secondly, we show that the dynamic response of the tree along the mean wind direction shows differences from that in the transverse direction, indicating the importance of studying both force components. Subsequently, the analysis is focused on the mean and maximum wind force over a wide wind speed range. During winter, both the mean and maximum force is described by a quadratic wind speed dependence, whereas during summer, an adjustment is needed to account for the reconfiguration of the leaves. This adjustment is parameterized using the same functional relationship for the mean and maximum force. Overall, in the wind speed range between 4–11 ms^{-1} the maximum wind load was 49%–66% and 52%–79% larger than the mean, during the summer and winter, respectively.

1. Introduction

Understanding the dynamic wind loading on trees both in the urban environment and in forests is of critical importance for calculating the risk of tree damage. Tree-fall or tree stem breakage in urban and peri-urban zones poses a threat for both human health and civil infrastructure and in forests can have important economic, social, and environmental impacts (Gardiner et al., 2010). One of the major difficulties in assessing the wind load is the challenge of making in-situ measurements of the wind force exerted on trees, which is one of the most central parameters for the study of the wind-tree interaction. Furthermore, the description of the physical processes that take place when wind flows through the crown of a tree still pose research questions that the scientific community needs to address to understand under which conditions tree damage occurs. A detailed review of the latest development in this research field with a focus on the damage of forest trees can be found in the work of Gardiner et al. (2016, 2019) and of Schindler et al. (2012). These studies highlight that one of the challenges in this research area is the inclusion of the biomechanical properties of trees, that play an important role in how trees respond under wind loading (James et al., 2014). In this context an accurate quantification of the both the mean and maximum wind force exerted on trees is necessary for both the validation and the further development of tree response models.

In the early 1970s, Hoag et al. (1971) and Mayhead (1973) provided the first results of experimental studies that investigated the response of trees and branches under wind loading. Having as a starting point the estimation of the drag coefficient of different tree species at a critical wind speed (Mayhead, 1973) and the understanding of the dynamic behaviour of tree branches, they observed that the wind force did not scale to the square of the flow velocity. For example Mayhead (1973) reports a linear correlation between force and wind speed, Hoag et al. (1971) observed that the force on olive tree brunches was proportional to the wind speed raised to a power of 1.4, while Roodbaraky et al. (1994) reported inconclusive results regarding the realistic values of the wind speed exponent. Vogel (1984) attributed this deviation to a characteristic response of the leaves under wind loading, which leads to a reconfiguration of their shape. He observed that this reconfiguration is not random, but is designed to minimize the exerted wind load. Due to the variations in shape and flexibility between leaves of different species, he introduced the *Vogel* parameter ($E \leq 0$) describing the force F proportionality to the wind speed U ($F \propto U^{2+E}$).

Since then several studies have been performed in order to investigate the mean response of a tree under a static applied load (Spatz and Bruechert, 2000) and the dynamic response under wind loads (Gardiner, 1994; Moore et al., 2005; Schindler et al., 2010, 2012, 2013). Studies with a focus on the mean load on a single tree have been

* Corresponding author.
E-mail address: nang@dtu.dk (N. Angelou).

https://doi.org/10.1016/j.jweia.2024.105966
Received 13 May 2024; Received in revised form 18 November 2024; Accepted 20 November 2024
Available online 13 December 2024

mainly performed in wind tunnels (e.g. Mayhead, 1973). However, due to size limitations, much of the wind tunnel experiments to date has been made under very artificial circumstances, on only parts of trees, small young trees (Gillies, 2002; Rudnicki et al., 2004; Vollsinger et al., 2005; Ishikawa et al., 2007; Manickathan et al., 2018; Tadrist et al., 2018), shrubby specimens (Cao et al., 2012) or scaled trees (Hao et al., 2020) and with rigid attachment to the ground. The majority of these studies report findings according to which the force does not scale as a quadratic function of the wind speed. These results are linked to a high degree of deformation, due to crown reconfiguration. However, considering the high flexibility of young trees and the very dense canopy of selected shrubby specimens (Cao et al., 2012), one can question to what extend the results of these studies are representative of a mature tree of the same species. Experimental studies, where the response of larger trees to wind load has been tested by placing tree limbs (Hoag et al., 1971) or young plantation trees (Kane and Smiley, 2006; Kane et al., 2008; Kitagawa et al., 2015) on moving trucks, have also reported deviations from the quadratic force to wind speed dependence. However, the anchoring of a tree on a platform and its exposure to a wind field with different features, in comparison to the one that the tree usually encounters during its growth, can also lead to a response that it is not characteristic of an open-grown, mature tree.

Full-scale measurements of wind loads on trees have been mainly performed on forest trees (e.g. Gardiner, 1994; Gardiner et al., 1997; Wellpott, 2008; Kamimura et al., 2022; Kolbe et al., 2022) with complex wind flow and with complex interactions with neighbouring trees. The few measurements that have been made on individual trees have measured tree and branch motion only (e.g. Barbacci et al., 2014). The estimation of the wind force exerted on living trees can be performed by monitoring the wind-induced response of a tree, which is typically achieved using sensors mounted on the stem. However, performing in-situ observations of the structural response of the tree is a challenging since the operation of tree-mounted sensors can be affected by the factors as the growth and the daily cycle of water transpiration of trees. This severely complicates the isolation of the wind signal in in-situ sensors.

An earlier study of the one-dimensional motion of an oak tree (Quercus robur) presented the first, to the authors knowledge, measurements of wind load on an isolated individual tree in its natural environment within a well characterized wind field (Angelou et al., 2019). In that study, it was shown how the wind-induced force signal could be isolated from the signals caused by effects of tree growth and daily temperature cycles. The resulting estimated mean force was subsequently confirmed in Angelou et al. (2021), where the momentum deficit of the wake of the tree, measured by multiple scanning wind lidars, was used to estimate the wind force. The results of the two methodologies agreed within 10%. In this paper we extend the analysis of the wind force exerted on the same tree to two dimensions. We conduct this investigation using field observations acquired during a field study that was performed in the framework of the *SingleTree* project,[1] which focused on the investigation of the wind conditions in the lee-side of solitary trees (Dellwik et al., 2019). In this work, we present a more complete picture of the loads exerted on a tree by investigating the relationship between the two-dimensional wind vector and the corresponding wind force exerted on a tree. This enables the assessment of the mean and maximum wind loading on this isolated tree over a wide range of wind speeds and directions both in winter (out-of-leaf) and in summer (in-leaf) and provides a baseline for our understanding of wind loading on trees in their natural environment.

[1] https://wind.dtu.dk/projects/research-projects/completed-projects/single-tree.

2. Material and methods

2.1. Experimental site

The field study focused on monitoring the wind-induced response of an open-grown, oak tree (*Quecus robur*) located on the East coast of the Roskilde fjord (32U, 694598E, 6175776N) within the Risø campus of the Technical University of Denmark (Fig. 1, left). The landscape around the tree can be described as a grassland and the closest plant vegetation is found at approximately 25 m to the East-southeast, where a low ridge with small shrub vegetation (<2.5 m) is located (for a detailed description see Fig. 2 in Dellwik et al., 2019). According to the local wind climate (see more in Appendix A), it is expected that the tree has grown while exposed to a persistent strong wind load, which have been originated mainly from the West. In that direction the tree is located approximately 56 m from the coast. The area between the coast and the tree is homogeneous and relatively flat, with a slope of ~2.4°. However, due to the roughness change (water-land), an internal boundary layer is expected to developed which impacts the vertical profile of the wind. The characteristics of vertical profile have been studied in Angelou et al. (2021) where it was found that the wind profile in the first 15 m above ground level (a.g.l.), is adequately described by the model proposed by Högström (1988).

The fact that deciduous trees drop their leaves during the winter enables the investigation of the impact of the foliage on the wind load exerted on the tree structure. Information regarding the geometry (Angelou et al., 2019), the optical porosity (Bekkers et al., 2022) and the plant area density (Dellwik et al., 2019) of the tree's crown was acquired using a laser terrestrial scanner (Leica Nova MS60, Leica Geosystems, Switzerland), both in the case of a bare and a fully developed crown. Based on those measurements, in the summer of 2016, the tree had a height (H) of 6.5 m and a crown that had an approximately homogeneous shape, with a maximum width equal to $w_x = w_y = 8.5$ m (see Fig. 2 (left)). The characteristic diameter at breast height (DBH) of the stem is measured to be equal to 29 cm. There is a slight asymmetry in the stem's cross-section. This asymmetry is consistent throughout the stem from the ground to the base of the crown, which was approximately at a height of 2 m (Fig. 2).

The estimation of the force on the tree was based on measurements of the wind-induced strain on the lower stem of the tree, using two strain gauges (CEA-250UWA-350, Micro Measurements, North Carolina, USA). Each strain gauge was installed on a caliper transducer following established methods of monitoring tree motion (Blackburn, 1997; Moore et al., 2005) (see Fig. 1(right) and Fig. 13 in Appendix B) and data was acquired at a sampling rate of 20 Hz. The horizontal angle between the unit vectors over which the two gauges measured the strain should ideally be equal to 90°, however due to practical limitations imposed by the trunk's morphology this angle was equal to 83° (see Fig. 2 (right)). The strain gauge measurements were calibrated and converted to a bending moment using multiple static pulling tests that took place during days with no wind (see more in Section 2.2 and Appendix B).

The measurements acquired by the strain gauges were analysed with respect to the local wind conditions. Two meteorological masts equipped with sonic anemometers (uSonic-983 Basic, Metek GmbH, DE), respectively, were used to monitor the wind conditions on the windward and leeward side of the tree at a 20 Hz sampling rate. The masts were equipped with two different configurations during the period of the field study. In the first period (June 2017–September 2017) only one sonic anemometer on each mast was used, installed at 4.0 m a.g.l which corresponded to $0.62H$. In the second period (September 2017–February 2018) the two masts were equipped with multiple sonic anemometers to provide information regarding the vertical wind profile on each side of the tree. The first mast (seen in background of Fig. 1(left) and denoted hereafter as M1) was installed towards the fjord and it was equipped with five sonic anemometers at the heights of

Fig. 1. Photographs of the open-grown oak tree and of the two meteorological masts used for monitoring the lee- and windward wind conditions of the tree (left) and of the caliper transducer of the strain gauge used to monitor the deformation of the stem (right).

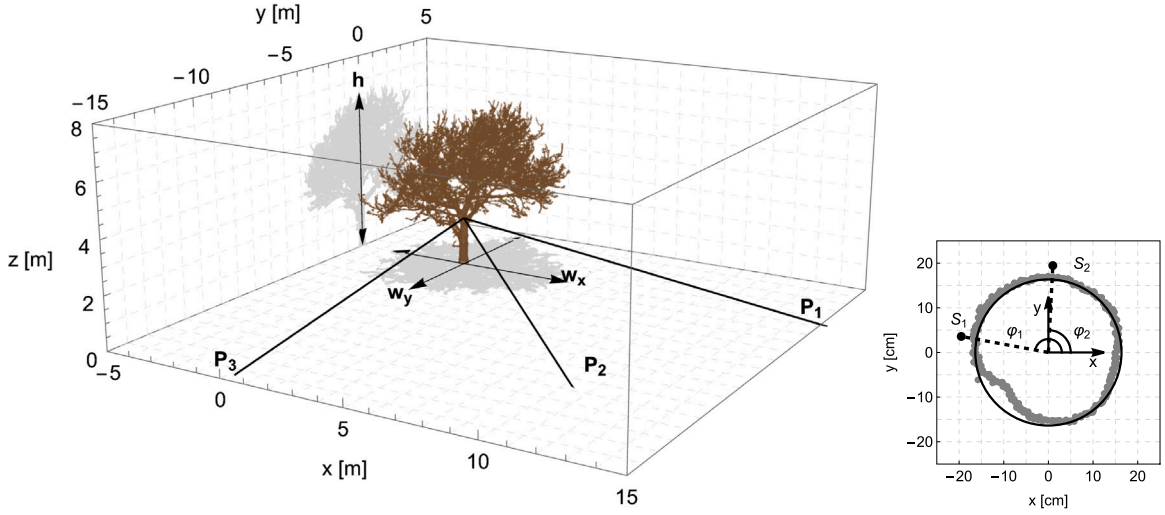

Fig. 2. Left: Perspective view of the tree during winter. The height H and the width of the crown along the longitudinal w_x and transverse w_y axes, relative to the wind direction of 290°, and the three directions of the pulling tests (P_1, P_2 and P_3) used for the calibration of the strain gauges are depicted. Right: Vertical cross section of the stem of the tree (depicted in grey) at 32 cm above ground, which presents the location of the two strain gauges (S_1 and S_2) and their corresponding direction relative to the x-axis (φ_1 and φ_2). In the plot there is also a black circle with a 16 cm radius, to visually present that the cross section of the stem is approximately homogeneous.

1.5 m ($0.23H$), 4.0 m ($0.62H$), 6.0 m ($0.92H$), 8.5 m ($1.31H$), 11.0 m ($1.69H$). The sonic anemometers were mounted on booms that pointed towards the direction of 200°, relative to geographical North. The second mast (seen in forefront of Fig. 1(left) and denoted hereafter as M2) was equipped with 10 sonic anemometers mounted on two booms, pointing towards the directions 20° and 200°, respectively. The heights of the booms of the M2 mast were at the same height a.g.l. as the M1 mast. A small offset (+0.15 m) had to be applied on the installation of the booms that pointed towards the North due to mounting limitations. Mast M1 was therefore measuring the upwind conditions and the M2 the downwind conditions when the wind direction was 290°. For this wind direction we did not expect any flow distortion of the sonic anemometer measurements due to the structure of the mast.

2.2. Horizontal wind force model

In order to formulate mathematically the relation between the amplitude and the direction of the horizontal wind force vector $\boldsymbol{F}$ and the wind conditions, we assume (i) that the force vector can be expressed a function of the wind-induced bending moments that result in tensile and compressive stresses in the lower part of the stem of the tree and (ii) any torsion on the tree structure and translation of the crown's mass centre can be considered negligible (Kolbe et al., 2024). Therefore, we use the strain deformation on the outer bark as a result of the bending moments about the longitudinal and transverse directions relative to the mean wind. We use the measurements of two strain gauges (denoted here s_1 and s_2), that are placed at the periphery of the stem of a tree at two directions, which are described by the two-dimensional, horizontal unit vectors $\hat{\boldsymbol{n}}_1$ and $\hat{\boldsymbol{n}}_2$, respectively.

The model is based on two further assumptions: (i) that the wind force can be considered as a single load exerted at the centre of gravity of the tree's crown, located at a height h and (ii) that the bending moments at the base of the stem can be approximately described by treating the tree as a vertical pole with a height h. Based on these two assumptions the wind force $\boldsymbol{F}$ that is exerted at a height h on a tree, will induce a bending moment $\boldsymbol{M}$ that is expressed as the outer product:

$$\boldsymbol{M} = \boldsymbol{r} \times \boldsymbol{F}, \tag{1}$$

where $\boldsymbol{r} = \{0, 0, h\}$ is the vector of the lever arm.

A strain gauge installed at the bottom of the stem of a tree measures the deformation due to the structural stress that is induced by the bending moment. The measurements can be expressed as the sum of the projections of the two bending moment components to the unit vector $\hat{\boldsymbol{n}}_i$, which denotes the direction of the installation of the strain gauge.

In the case of the two strain gauges s_i $(i = 1, 2)$ used in this study, this can be written as:

$$s_i = c_i \left(M_x \cdot \cos\varphi_i + M_y \cdot \sin\varphi_i \right) \text{ with } i = 1, 2, \tag{2}$$

where c_i is a calibration factor that describes the bending moment to strain conversion and φ_i is the horizontal direction of the vector $\hat{\boldsymbol{n}}_i$ for each of the two strain gauges. By substituting Eq. (1) to Eq. (2) a strain gauge s_i measurement is expressed as function of the two components of the force:

$$s_i = c_i \left(-F_y \cdot h \cdot \cos\varphi_i + F_x \cdot h \cdot \sin\varphi_i \right) \tag{3}$$

Therefore in the case of a horizontal wind vector, by neglecting the effect of both the translation of the crown's mass centre and the torsional moment on the stem, we can use Eq. (2) to express the two components of the force as:

$$F_x = \frac{a_1 \cdot s_2 - a_2 \cdot s_1}{(a_1 \cdot b_2 - a_2 \cdot b_1)h} \tag{4}$$

and

$$F_y = \frac{b_1 \cdot s_2 - b_2 \cdot s_1}{(a_1 \cdot b_2 - a_2 \cdot b_1)h}, \tag{5}$$

where the parameters a and b correspond to the product of the strain gauge sensitivity c_i with the trigonometric functions as:

$$a_i = c_i \cdot \cos\phi_i \text{ and } b_i = c_i \cdot \sin\phi_i \text{ with } i = 1, 2. \tag{6}$$

When the tree acts like a bluff body then the force exerted over the crown area A, with a force coefficient c_d is expressed as a function of the magnitude of the wind vector $\boldsymbol{U}$ at the centre of gravity of the canopy:

$$|\boldsymbol{F}| = \frac{1}{2}\rho c_d A |\boldsymbol{U}|^2, \tag{7}$$

which can be expanded to the two horizontal components as:

$$F_x = \frac{1}{2}\rho c_d A |\boldsymbol{U}|^2 \frac{U_x}{|\boldsymbol{U}|} \text{ and } F_y = \frac{1}{2}\rho c_d A |\boldsymbol{U}|^2 \frac{U_y}{|\boldsymbol{U}|}, \tag{8}$$

where U_x and U_y are the two components of the wind vector, $|\boldsymbol{U}| = \sqrt{U_x^2 + U_y^2}$ is the amplitude of the horizontal wind vector and ρ is the air density. However, as it is shown by Vogel (1984), flexible elements of tree (e.g. leaves) tend to streamline under wind load. In that case the force to wind speed relationship departs from the square dependency, therefore we can write this as:

$$F_x = \beta |\boldsymbol{U}|^{E+2} \frac{U_x}{|\boldsymbol{U}|} \text{ and } F_y = \beta |\boldsymbol{U}|^{E+2} \frac{U_y}{|\boldsymbol{U}|}, \tag{9}$$

where E is the Vogel exponent, a parameter that represents the ability of a structure to streamline under wind load and the pre-multiplier β that is dependent on both the exponent E and the magnitude of the wind speed in order to satisfy the units of the force. The Vogel exponent can have values between 0 (corresponding to a force exerted on a bluff body) and −1 (corresponding to a force that is linearly dependent on the wind speed). A physical expression of Eq. (9) has been presented in the work of Gosselin (2019), which requires that the area and the force coefficient of a tree are wind speed dependent parameters. Examples of mathematical formulation of this relationship have been discussed by Whittaker et al. (2013) and Bekkers et al. (2022) in the case of the reconfiguration of plants and trees, respectively.

As it is described in Angelou et al. (2019), the strain gauge measurements (s_m) are biased by temperature (s_t) and time-dependent zero-offset long-term drifts (s_0). Therefore, the measurements of a strain gauge (s_i) can be expressed as the sum of the wind induced strain (s_w) and the two aforementioned drifts.

$$s_m = s_w + s_t + s_0 \Rightarrow s'_m = s_w + s_0 \tag{10}$$

where $s'_m = s_m - s_t$. For the estimation of s_t the same temperature sensitivity (i.e. 0.034 mV/°C) was used throughout the field campaign. The value of s_t was estimated by monitoring the fluctuations of the strain gauge signals during days with no wind and by relating those to the temperature reading of the sonic anemometer at 4 m at the upwind mast M1. In order to convert the signal of two strain gauges to the two components of the wind force using Eqs. (4) and (5), we have to first estimate the c_i parameter of Eq. (2) and subsequently estimate the time-dependent zero-offset drifts of each of the two strain gauges. The former is part of the strain gauge calibration procedure, which is presented in Appendix B and was based on the application of a static load from two different directions.

In order to assess the accuracy of the calibration we applied a load from an additional, randomly selected direction (see more in Appendix B) and compared the applied load with the reconstructed one. The results of this comparison are presented in Fig. 3, which shows a very good agreement of the magnitude and direction between the applied (F_m, θ_m) and reconstructed (F_e, θ_e) load. In the top plot of Fig. 3 we show the applied static load that was used to assess the calibration of the two strain gauges. The load reached 2500 N, with varying steps of approximately 500 N. Each load was applied for approximately 100 s. We observe that the difference between the applied and the estimated loads is less than 100 N, corresponding to differences of less than 5%, irrespective of the magnitude of the applied load. The reconstructed horizontal vector is also found to be aligned to the applied vector, since we find differences of less than 2% between the two. Larger values are related to the abrupt responses of the tree structure which occur at the beginning and at the end of the static load application.

Regarding the time-dependent zero-offset s_o, for its estimation we followed the same methodology presented in Angelou et al. (2019). For this purpose, we express the strain s'_m as a function of wind speed. By combining Eqs. (2) and (9) in Eq. (10) we derive the following expression:

$$s'_{m,i} = c_i h \beta |\boldsymbol{U}|^{E+1} \left(-U_y \cdot \cos\phi_i + U_x \cdot \sin\phi_i \right) + s_{0,i} \quad \text{where } i = 1, 2. \tag{11}$$

Using s_m, U_x and U_y and the estimated values of Eq. (2) from the static pulling tests we find the values of β, E and s_0 that minimize the error between the observations and Eq. (11). This step is performed using 1-min mean values. The selection of this time scale is based on the findings of Angelou et al. (2019). Once the estimation of the zero offsets is done, then the two-dimensional force vector is performed using Eqs. (4) and (5).

2.3. Wind conditions

The measurement campaign took place between June 2017 and February 2018. The leaves of the tree fall within a period of three weeks in October. Therefore, we consider data that are acquired between June to September as descriptive of the tree with a fully-developed crown with leaves (and hereafter we denote that tree state as the *summer tree*) and data acquired between November to February as descriptive of a leafless tree (and hereafter we denote that tree state as *winter tree*). During this seven-month period, we have selected for the analysis 1550 and 663 10-min periods, for the case of the summer and winter tree respectively. These periods were selected based on the criterion that the mean direction should be within the sector 275°–305°. The resulting data set was characterized by mean wind speeds within the range 4–11 m s^{-1}. For the estimation of the speed and direction of the wind the sonic anemometer measurements at 4 m, above ground, were used. A bar-chart with the number of periods per different wind speeds is presented in Fig. 4. The turbulence intensity (TI), defined as the ratio between the mean horizontal wind speed and the corresponding standard deviation, was equal to 0.14 ± 0.02 and 0.12 ± 0.02 for the summer and winter cases respectively. These TI levels are moderate and typical over a flat landscape. For the summer cases the TI was wind speed independent, as seen in Fig. 4. However in the winter case we find slightly higher values of TI at higher wind speeds. These observations could be attributed to both the atmospheric stability conditions and to terrain characteristics in the upwind direction. Regarding the atmospheric stability, the height

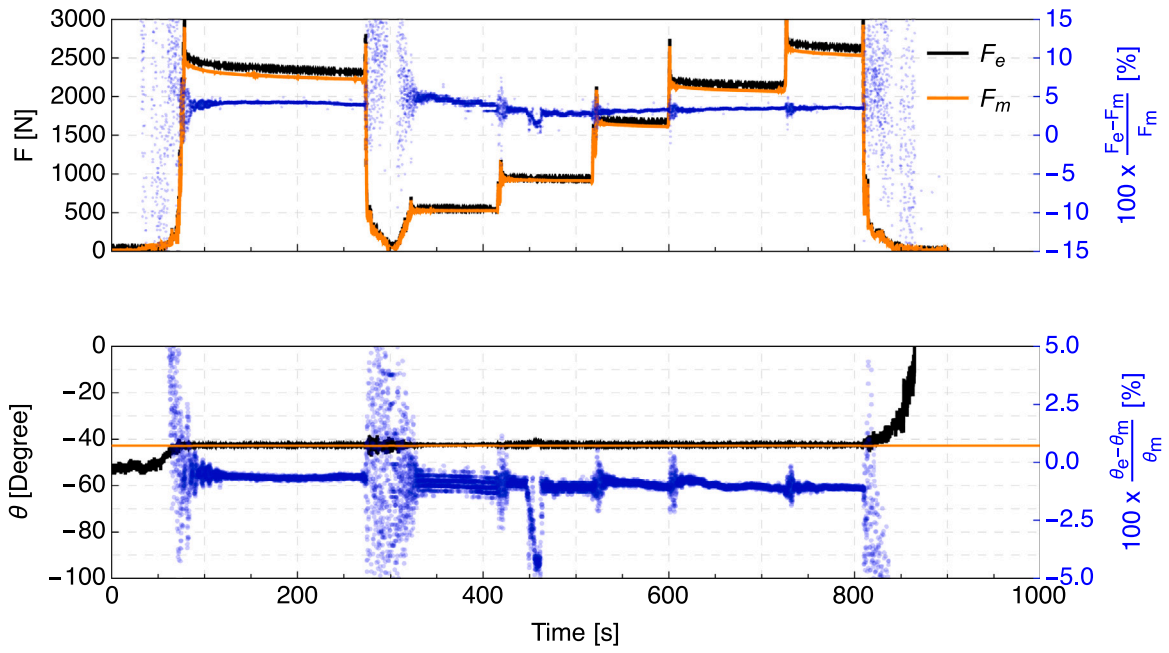

Fig. 3. Measured F_m (orange) and estimated F_e (black) magnitude (top plot) and direction (bottom plot) of the applied static load, along with the relative difference in percentage (blue) between the two quantities.

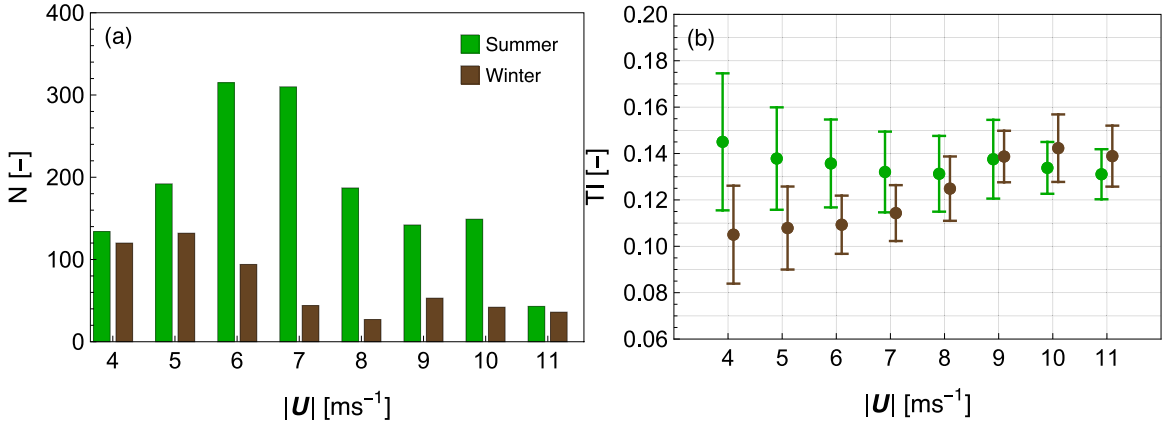

Fig. 4. (a) Number of 10-min periods used in the analysis and (b) turbulence intensity (TI) values for different 1 m s^{-1} wind speed bins, for the summer and winter.

normalized Obukhov length z/L values (Wyngaard, 2010), estimated using the sonic anemometer measurements at 4 m, indicate that the atmospheric stability of the selected cases during both the summer and winter, was neutral. However, the z/L values were closer to the stable limit (i.e. $z/L \sim 0.1$) in the winter, which could partially explain the lower TI values. Furthermore, during the winter the grass field in the upwind direction of the tree has a lower height than in the summer. The difference can reach 50 cm, which could also contribute to the observed slightly higher TI values in the summer.

In Fig. 5 we present the power spectral densities, defined as the absolute square of the Fourier transform of the longitudinal u and lateral v components of the horizontal wind vector, in different wind speed ranges. For the estimation of the power spectral densities we use the sonic anemometer observations acquired at 4 m above ground. We observe that both in the summer and the winter period the characteristics of the power spectral densities are not typical of atmospheric turbulence in the surface layer (Kaimal et al., 1972). The two main differences are first that there is no distinct peak in the spectra of either horizontal wind components. This could be attributed to low frequency mesoscale turbulence fluctuations are typically observed in the wind conditions offshore (Larsén et al., 2016; Syed and Mann, 2024). Furthermore, in the inertial sub-range, the energy of the turbulent fluctuations deviate from the expected −2/3 slope (depicted by a dashed line in each plot). Our hypothesis is that this is attributed to noise in the measurements of the sonic anemometer, the amplitude of which has been reported that is dependent on the relative direction of the boom and the wind direction (Peña et al., 2019).

3. Results

3.1. Tree response

In order to quantify the mean and maximum wind loads on the tree, we need to know over which time scales the response of tree can be related to the turbulent fluctuations reported in Fig. 5. We present in Fig. 6 the ratio of the power spectral densities of the horizontal fluctuations of the force $\{F_x, F_y\}$ and of the corresponding components of the wind vector $\{U_x, U_y\}$, which are defined in the coordinate system presented in Fig. 2. For this purpose we denote the ratio of the power spectral densities as the *spectral transfer function* between the single-point turbulence spectrum at the centre of the crown and the wind-induced force. Fig. 6 shows the spectral transfer function in both

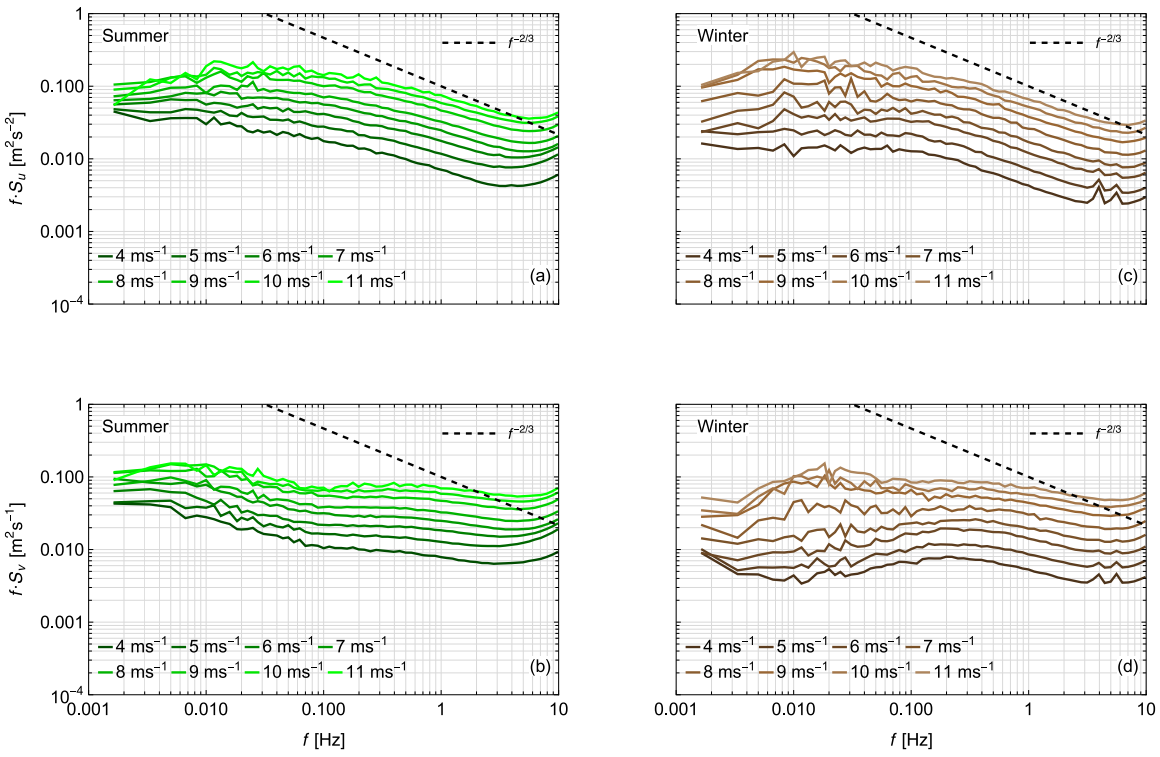

Fig. 5. Power spectral densities of the longitudinal ((a) and (c)) and lateral ((b) and (d)) components of the wind vector at 4 m above the ground for the summer (left column) and winter (right column) period of the field campaign. The dashed line in all four figures correspond to the −2/3 slope.

the x and y direction for different wind speeds ranging from 4 to 11 m s^{-1}, measured in summer and in winter.

In both the summer and winter we observe that the transfer function of both x and y components is approximately constant over the low frequency bandwidth, that extends from 0.0016 Hz to 0.016 Hz. This frequency range corresponds to fluctuations with a period from 1 to 10 min. We can thus consider the tree motion at the frequencies up to 0.016 Hz as quasi-static in which a displacement of the tree stem is linked linearly to the wind speed. Beyond that point the transfer function decreases until the frequency range 0.8–1.1 Hz where a peak is present in all components. The peak is more easily visible in the winter tree, with a peak appearing between 1–2 Hz. Furthermore, the peak is slightly more dominant in the y-axis than the x-axis. Similar trends have been reported by Schindler et al. (2013) in the case of a deciduous broad-leaved tree. The peak is related to the natural frequency of the tree structure which in the case of open-grown broad-leaf trees is typically found to be less than 2 Hz (Jackson et al., 2021). Finally, we observe a decrease in the transfer function after 2 Hz, which relates to the fact that small frequency wind perturbations do not have an impact on the tree response at the base of the stem.

In general, the stronger the wind speed the higher the spectral transfer function. This is attributed to the parameterization of the force which in the case of a bluff body is typically expressed by the square of the wind speed. Furthermore, the higher the wind speed the lower the slope of the F_x in the frequency bandwidth between 0.02 and 0.5 Hz, in the case of both the summer and winter tree. This means that the trees tends to respond in a more static way as the wind load increases and thus the higher the wind speed the more correlated are the fluctuations of force with the ones of the wind speed over a broader frequency bandwidth.

An example of the estimated values of the two components of the horizontal force vector is presented in Fig. 7, corresponding to cases where the 10-min mean wind direction had a 13° offset from it. Fig. 7 shows the 20 Hz horizontal force vector, denoted by $\{F_{x,0.05s}, F_{y,0.05s}\}$, during two 10-min periods characterized by two mean wind speeds of 5 and 9 m s^{-1}, for both the case of the summer and winter tree. We observe that in the case of the winter tree the fluctuations of the force vector take place aligned with the mean wind direction (depicted by a red arrow). Furthermore, when the wind speed is equal to 9 m s^{-1}, we observe more extreme values of F_x compared to values when the wind speed equals 5 m s^{-1}. This can be seen visually from the plot where the ratio $F_x/|\boldsymbol{F}|$ occasionally reaches values higher than 1.5. On the contrary, in the case of the summer tree, we observe less extreme values, but also more spread in the transverse direction. In all cases, the fluctuations of the two components of the force vector are offset from 0 N. The mean value of two components is highlighted by a red dot in each plot, which shows that the axis over which open-grown trees sway is displaced following the direction of the mean wind (depicted by a black arrow). Similar findings have been reported in the work of James et al. (2006), where they show that trees with a slender crown form tend to sway along a vertical reference axis, while trees with a broad crown form, typical of open-grown trees, tend to sway along an axis displaced by the mean wind direction. Furthermore, the observed two dimensional distribution of the force is different also from the results presented in Hassinen et al. (1998), who shows the stem displacement of a Scots pine located at a forest edge. Even though the values are not centred at 0, they report that there is a larger lateral displacement than longitudinal, relative to the mean wind direction. The observed tree response of the open-grown tree is also different from forest trees even in the case of extreme high wind speeds, for example of forest trees during a typhoon (Kamimura et al., 2022).

3.2. Mean two-dimensional wind force

The estimation of the mean horizontal force that was exerted on the tree was performed using Eqs. (4), (5) and (3) based on 1-min mean measurements. Fig. 8(a) shows a scatter plot of the estimated force amplitude $F = |\boldsymbol{F}| = \sqrt{F_x^2 + F_y^2}$ as function of the horizontal wind speed $U = |\boldsymbol{F}| = \sqrt{U_x^2 + U_y^2}$, using 15 500 and 6526 1-min values for the summer and winter, respectively. In order to quantify the F vs. U

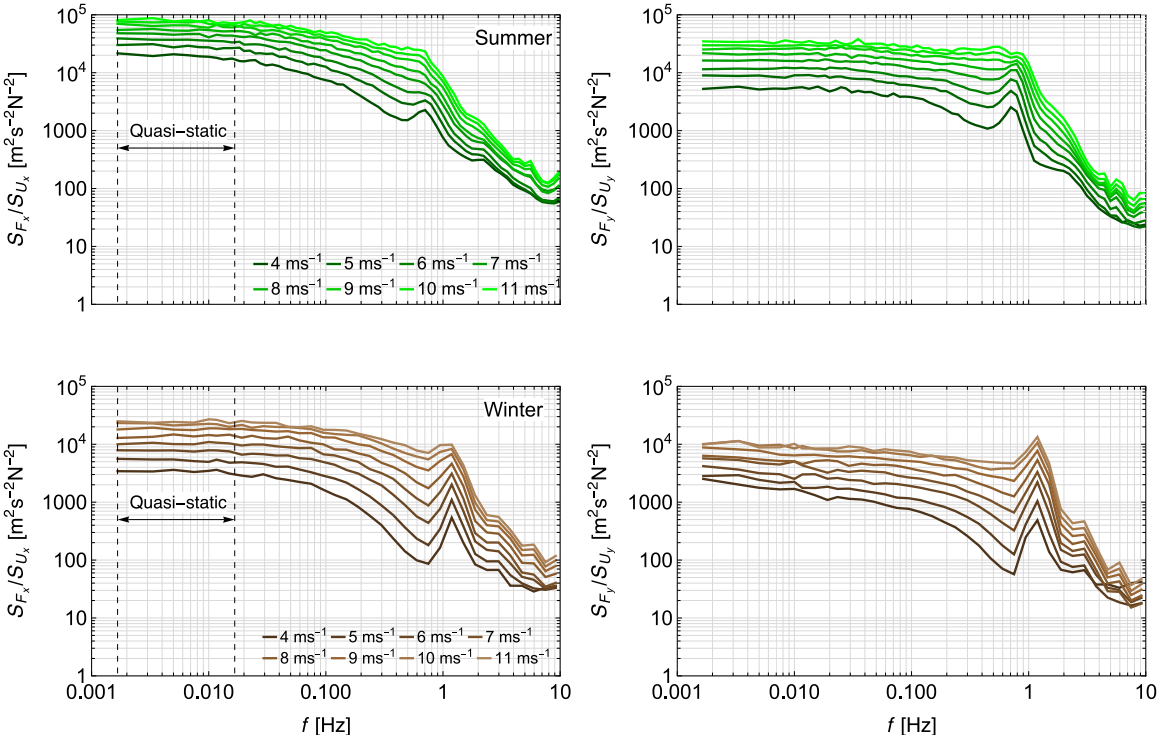

Fig. 6. Ratio of the power spectral densities of the horizontal fluctuations of the force and of the corresponding component of the wind vector for different wind speed, measured for two tree states, summer (green shaded curves, top row plots) and winter (brown shaded curves in bottom row plots).

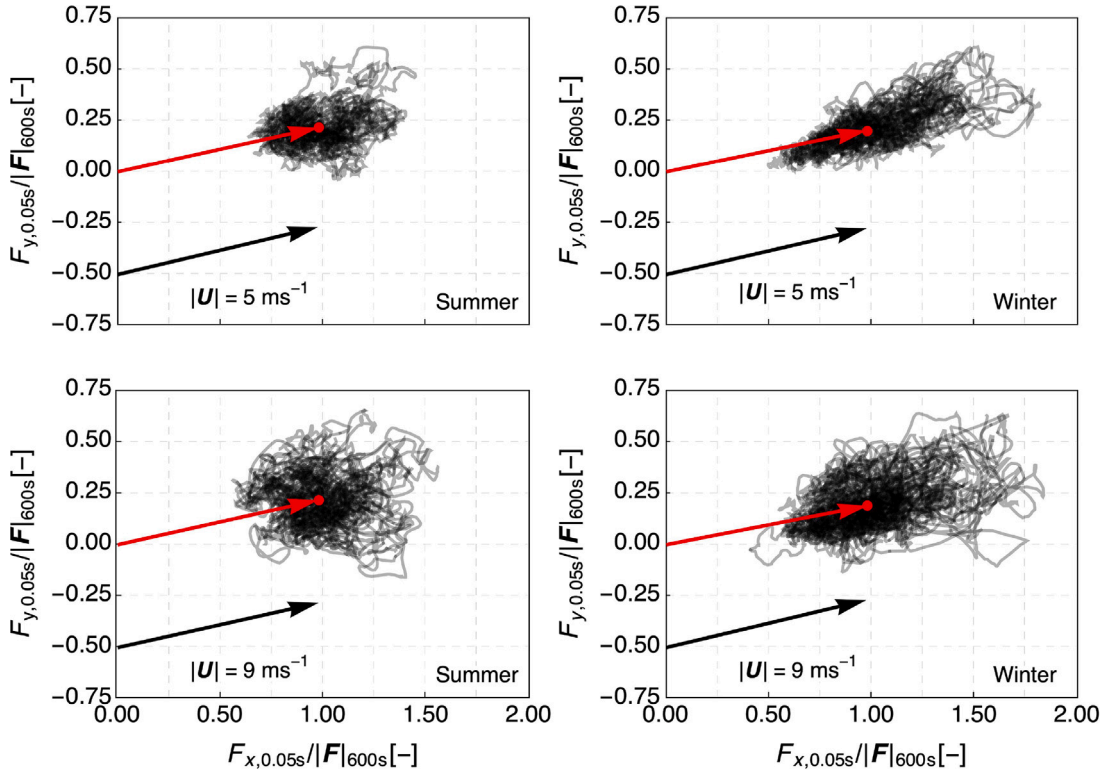

Fig. 7. Examples of the trajectory of the horizontal force vector during different 10-min periods when the mean wind speed was either 5 m s^{-1} (top row) or 9 m s^{-1} (bottom row) for summer (left column) and winter (right column) periods, respectively, when the wind direction had an offset of 13° relative to the x-axis. The values of the two components are normalized by the mean wind force. The black arrow corresponds to the mean wind direction and the red arrow highlights the direction of the coordinates of the mean F_x and F_y.

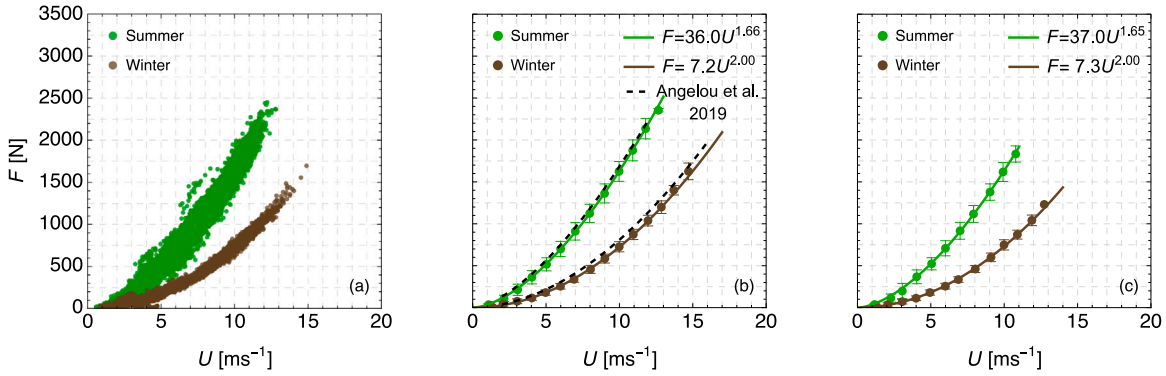

Fig. 8. (a) 1-min mean force vs. wind speed for the case of the winter (depicted in brown dots) and summer (depicted in green trees) tree. (b) 1-m s^{-1} and (c) 10-m s^{-1} bin averaged values. The error bars correspond to one standard deviation about the mean.

we apply a non-linear model fit with a function $y = \beta x^{E+2}$ using values averaged over 1-m s^{-1} bins, which is presented in Fig. 8(b). For the estimation of E we constrain the value of the Vogel exponent to be between 0 and −1 corresponding to the extreme cases of a bluff and a streamlined body, respectively. We find that the force on a oak tree during the winter is described by a quadratic wind speed dependence (i.e. $E = 0$), meaning that the tree can be approximated as a bluff body. However, during the summer when the tree's crown is fully developed with leaves the dependence of force on wind speed is described by a Vogel exponent E equal to −0.34. These findings are in agreement with the results presented in Angelou et al. (2019) (see black dashed curves in Fig. 8(b)), where an one-dimensional analysis of the horizontal force on the same tree was performed. In that study, the focus was on the cases where the wind direction was aligned to the axis where the single strain transducer was measuring the deformation of the stem. We find that the amplitude of the two-dimensional force vector is on average 1% and 11% lower than the one-dimensional, in the summer and winter, respectively. We attribute the observed difference partially to a more optimum estimation of the temperature contribution (s_t) on the strain gauge measurements and partially to temporal drifts of the calibration coefficient c. In order to check the sensitivity of the results on the averaging time scale we performed the same analysis using 10-min mean values. Fig. 8(c) presents the results, where we observe that we not only find the same F vs. U dependence, but also the statistically uncertainty, expressed by the error bars in the figure which correspond to the standard deviation about the mean, is similar when using either 1-min or 10-min values. Overall, the mean force during the summer is 90% to 190% higher than that during the winter, in the wind speed range between 5 and 15 m s^{-1}. This difference between the summer and winter is in agreement with the increase in the plant area density of the crown without and with leaves, as reported for the tree examined here in the study of Dellwik et al. (2019).

Furthermore, we find that the assumption of the isotropic response of the tree along the x and y axes, expressed in Eqs. (8) and (9), gives reasonable results, since the estimated Vogel exponent values, for the summer and winter tree, describe well both the longitudinal and transverse components of the force. Fig. 9 presents the 1-min mean values of the F_x and F_y as a function of $U_x|\boldsymbol{U}|^{E+1}$ and $U_y|\boldsymbol{U}|^{E+1}$, when E was set equal to −0.35 and 0, respectively. To assess the sensitivity of the estimated values of the horizontal components of the force on the Vogel exponent we present in Appendix C the wind force to wind speed dependence assuming a Vogel exponent (E) equal to −1 ($F \propto U$) and 0 ($F \propto U^2$). The figure shows the deviations between the model and the measurements. For example, by assuming a quadratic relationship, corresponding to a bluff body, we can underestimate the mean force by more than 20% when the wind speed is higher than 12 m s^{-1}.

The estimated values of the mean force presented in Fig. 8, can be used in Eq. (7) to calculate the drag coefficient of the tree. In the case of the summer tree, this requires the consideration that the frontal area of the crown and the drag coefficient are wind speed dependent, as has been demonstrated for example in the works of Rudnicki et al. (2004), Manickathan et al. (2018) and Bekkers et al. (2022), which is out of the scope of this article. However, we study the drag coefficient in the case of the winter tree, since we find that the wind-induce force on an oak tree without leaves, scales with the square of the wind speed. For this purpose we use two values of the frontal area. According to Bekkers et al. (2022), who applied an image processing of a series of photographs of the tree, this should be equal to approximately 25 m^2 and according to the laser scanner point cloud measurements this should be equal to approximately 20 m^2. Using these two values and by assuming that air density was equal to 1.225 kg m^{-3} we estimate the force coefficient of a leaf-less oak tree to have a value between 0.46 and 0.57. These values are 33% to 48% lower than the drag coefficient value (c_d = 0.89) estimated for the same tree during the summer when the crown was fully leaved and for a wind speed of 5 m s^{-1} (see more in Bekkers et al., 2022). The drag coefficient range of values found for the winter period are higher than values reported in the work of Manickathan et al. (2018) for the case of a defoliated holly (Ilex crenata) tree.

3.3. Maximum two-dimensional wind force

The estimation of the maximum aerodynamic force was performed using either the maximum 3-second moving average (Method 1) or the most frequent maximum values of the 20 Hz data (Method 2) over a given period of time. Method 1 is based on the definition of the 3-second wind gust, which has been historically a common choice in wind engineering research and applications for the estimation of extreme wind speeds (Lombardo, 2021). To perform this calculation the 3-second moving average of the 20-Hz time series of the force over a period was estimated and subsequently the maximum value was selected. Method 2 is based on finding the most common of the maximum values that occur over consecutive segments of a time period. In our case, we first split the acquired 20-Hz data into 20 equal periods, subsequently we find the maximum value of each period and finally we select the most common maximum value (modal value). This method, presented by Lieblein (1976), has been applied for the estimation of the maximum bending moments on trees (e.g. Wellpott, 2008; Hale et al., 2012). Traditionally the maximum values are estimated over 10-min periods, in an attempt to relate extreme velocity values to the mean of the background flow. This calculation relies on the assumption

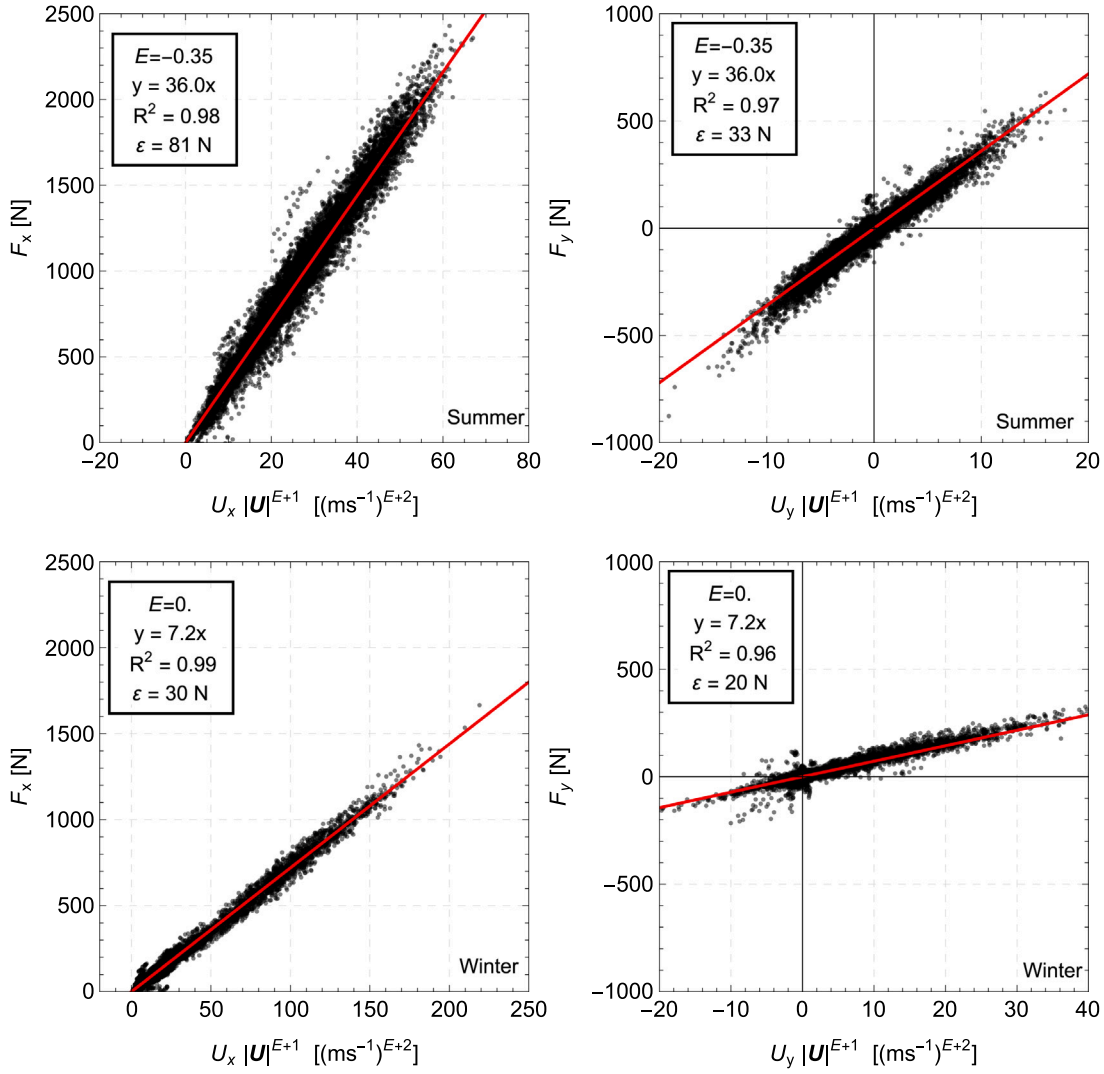

Fig. 9. Mean longitudinal (left column) and transverse (right column) force during the summer (top row) and winter (bottom row) period. The data used correspond to 1-min values, where E is equal to −0.35 and 0 for the summer and winter period, respectively.

that the flow over 10-min can be considered as stationary. However, atmospheric flows are rarely stationary, and thus in order to investigate the impact of the duration of the averaging period, it is valuable to relate the maximum values to different mean time scales. Furthermore, in the field studies of the maximum wind loads exerted on forest trees and due to practical limitations, the reference wind measurements are not necessary co-located with the tree under investigation. Therefore, in order to minimize the error associated with the temporal variations of the wind, long time intervals are used to estimate the mean wind speed. Thus, in order to study the sensitivity of the estimated maximum values on the statistics of the background mean wind flow, we calculate the maximum statistics over four different duration periods equal to 1, 10, 30 and 60 min.

Fig. 10 presents the estimated maximum values of the two methods, for both the summer and winter, to allow a comparison of the results. We observe that during the winter the maximum values scale with the square of the wind speed, irrespective of the method used (see Fig. 10(d) and (e)). The maximum values from Method 1 are 20–30% higher than the ones from Method 2 (Fig. 10(f)), in the wind speed range between 5 m s^{-1} and 20 m s^{-1}. During summer, when estimating the maximum values in relation to the 1-min mean wind speed, we find a Vogel exponent similar to the mean force (i.e. $E = -0.35$ in Method 1 and $E = -0.32$ in Method 2), as presented in Fig. 10(a) and (b). As we would expect, the shorter the period the larger the mean wind speed relative to the corresponding maximum value, which results in a smaller pre-multiplier in the relationship between the force and the mean wind speed and in a lower value of E. Overall, in the case of the summer tree, we find that Method 1 gives on average 16–20% higher values than Method 2 (Fig. 10(c)). Due to the observed variation of the pre-multiplier and the wind speed exponent E that describe the maximum force parameterization (see legends in Fig. 10(a) and (b)), the difference between the estimated maximum force from the two methods is wind speed dependent (Fig. 10(c)). The largest differences are found in the low mean wind speed region (i.e. < 5 m s^{-1}). The difference between the two methods in the summer converges when the mean wind speed is 10 m s^{-1} and beyond that limit we find that the difference between the two methods in the case of the summer tree is similar to the one found in the case of the winter tree, when the averaging period is either 1 min or 10 min. For longer averaging

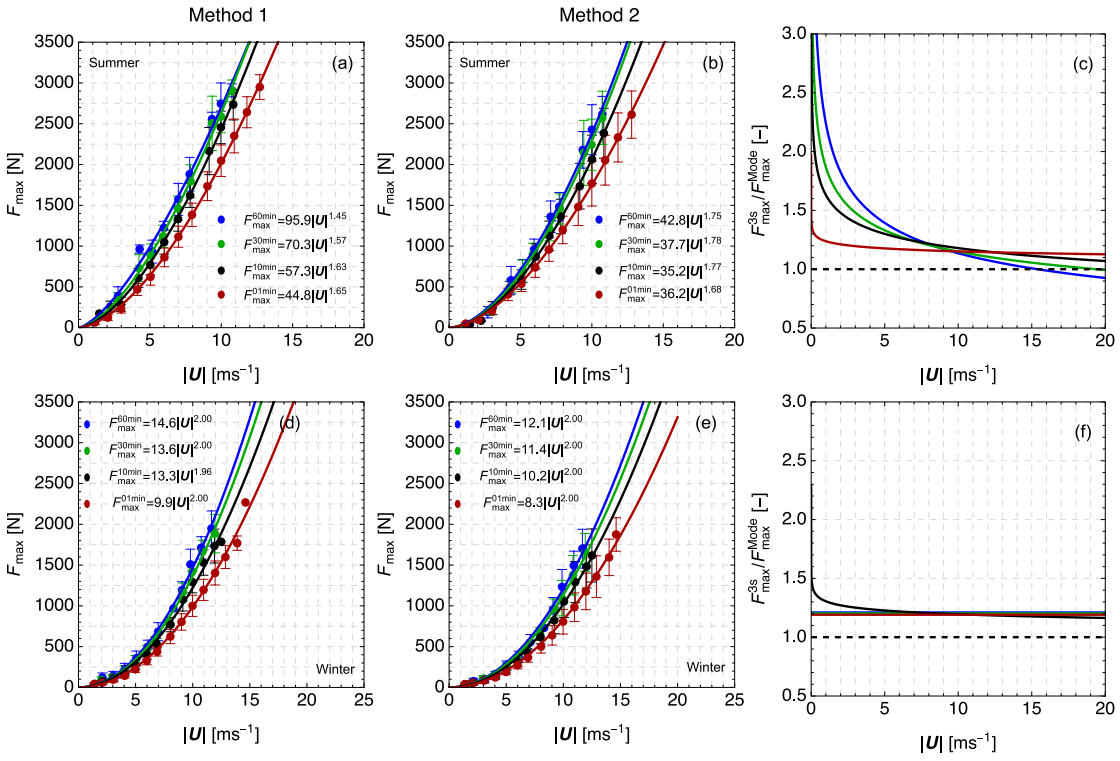

Fig. 10. Maximum aerodynamic force F_{max} estimated based on either the maximum 3-second moving average (Method 1) or the most frequent maximum values over different periods with a duration equal to 1, 10, 30 and 60 min (Method 2). The maximum values are presented in figures (a), (b), (d) and (e) as a function of the mean wind speed of each period for the case of both the summer and winter tree. Figures (c) and (f) present the ratio between the estimated maximum values of the two methods per wind speed in the summer (c) and winter (f).

periods we observe negligible deviations between the two methods when the wind speed is above 15 m s^{-1}.

Overall, we observe that the maximum force exerted on the tree in the summer is between 171% to 26% (Method 1) or 160% to 40% (Method 2) larger than the one in the winter. The higher differences correspond to the lower wind speed range (~5 m s^{-1}) and there is a decreasing trend with increasing wind speed. The differences found in the maximum force between the summer and the winter period are in the same range as the difference between the one found for the case of the mean force (see Fig. 8). As an example we present in Table 1 a comparison between the mean and the maximum wind force for the wind speed range between 4 and 11 m s^{-1}. The mean values correspond to the ones estimated over 10-min periods, while the maximum values correspond to the ones estimated using Method 1 over 10-min periods. The selection of the 10-min periods is based on the fact that this duration is typically being used to derive mean wind statistics. We can see that during the summer the maximum force is 45%–66% higher than the mean. The corresponding percentage for the case of the winter tree is slightly higher with values between 52%–79%. When comparing mean and the maximum wind force between the summer and the winter period we observe that the relative difference in both the mean R_{mean} and the maximum R_{max} has a decreasing trend with increasing wind speed.

To our knowledge, the results presented in Figs. 8 and 10 are the first concurrent estimations of the mean and maximum force on an open-grown tree. Even though open-grown trees have different physical characteristics to forest trees (*e.g.* crown size and stemp temper) and they are exposed to wind conditions with different characteristics, we attempt here to discuss the results of the maximum estimated values with respect to the results presented in the work of Wellpott (2008) and Hale et al. (2012). Hale et al. (2012) acquired wind loading measurements on trees with varying physical characteristics in four different forests, using calibrated strain gauges installed on the stem of trees. They found a linear relationship between the maximum hourly turning moment and the square of the average hourly wind speed at the canopy top. Furthermore, based on their findings, the maximum bending moment values varied from 0.8 kNm (in the case of a Kershope tree of 15-m height) to 30 kNm (in the case of a Clocaenog tree of 31-m height) at 7 m s^{-1} Hale et al. (see Fig. 1 in 2012). In the same wind speed range, Wellpott (See Fig. 5 in 2008), assuming again a quadratic relationship between force and wind speed, report maximum

Table 1
Table of the mean F_{mean} and maximum F_{max} wind force exerted on the tree during the summer and winter period. In the parenthesis is presented the relative increase of the maximum force in relation to the mean for each wind speed. The two last columns at the right present the relative percentage $(F_{summer} - F_{winter})/F_{winter} \times 100$ of the mean R_{mean} and maximum load R_{max} difference between the summer and winter tree. The values correspond to the ones estimated over a 10-min period and the maximum wind force corresponds to the results of the Method 1 (i.e. using the maximum 3-second moving average).

U [m s^{-1}]	Summer tree		Winter tree		R_{mean} [%]	R_{max} [%]
	F_{mean} [N]	F_{max} [N]	F_{mean} [N]	F_{max} [N]		
4	368	610(66%)	112	173(54%)	228%	253%
5	523	772(48%)	180	274(52%)	191%	182%
6	708	1048(48%)	256	403(57%)	177%	160%
7	916	1331(45%)	335	537(60%)	173%	148%
8	1118	1622(45%)	461	770(67%)	142%	111%
9	1378	2165(57%)	600	1076(79%)	130%	101%
10	1618	2455(52%)	748	1293(73%)	116%	90%
11	1832	2734(49%)	871	1530(76%)	110%	79%

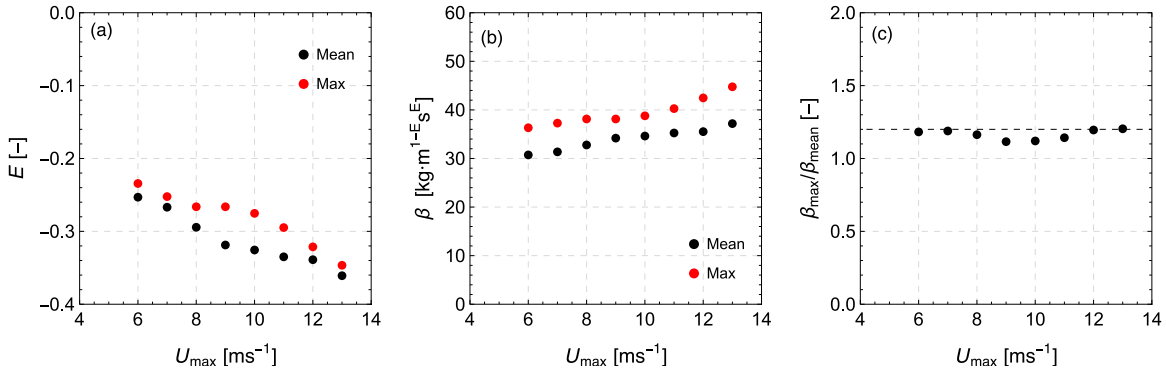

Fig. 11. Vogel exponent (a) and pre-multiplier (b) values of the parameters of the function $y = \beta x^{E+2}$ for the mean, depicted in black, and maximum (Method 1), depicted in red, force versus different wind speeds that range between 0 m s^{-1} and Umax over 1-min periods. The Umax is ranging from 6 to 13 m s^{-1}. The ratio between the maximum and mean pre-multiplier values is presented in (c) for the different wind speed ranges.

loads 10 and 150 kNm in a study of nine Sitka spruce (Picea sitchensis) trees with heights between 20 and 30 m, that were located in a forest stand. In the case of our tree and using the estimated function of maximum force for the summer tree for the 1-h period, we find that the corresponding maximum bending moment at 7 m s^{-1} is equal to 5.2 kNm and to 6.4 kNm for the case of the summer tree, using Method 1 and 2, respectively. This shows that despite the on average smaller size of open-grown trees, they experience similar extreme bending moments as trees in forests.

4. Discussion

Field studies of the wind force on trees have the advantage of examining the wind and tree interaction in natural conditions. This is important since it facilitates a realistic observation of the tree response. However, field studies also pose two challenges. First, the wind conditions cannot be controlled and, additionally, a tree in nature responds to all environmental conditions, not only the wind. Hence, the impact of the biological processes on the wind load observations has to be taken into account. For example, the diurnal transpiration cycle, which cause the stem to swell during day-time, affects the stem-mounted strain transducers (Chap. 4 in Blackburn, 1997). Furthermore, freezing winter conditions could result in a stiffer wood (Chap. 5 in Blackburn, 1997). These environmental conditions are difficult to be reproduced in a scaled study in a wind tunnel. Furthermore, scaled studies of the tree response are often performed by either cutting trees and therefore neglecting the effect of the root-system or by selecting young trees that they can fit in wind tunnel facilities. Here, we take into account the effect of these variables, by first applying a calibration of the strain gauge transducers in different periods and therefore investigating the effect of the tree growth on their calibration, but also of the effect of the root system in different periods. The calibration is performed in each transducer separately since, as we show in Appendix B the sensitivity of a strain gauge is varying in different locations around the stem. Furthermore, we estimate the zero offset of the strain gauge for every 1-hour period separately and thus incorporate in that term the effects that diurnal and ambient conditions have on the tree-strain gauge system.

One of the contributions of this study is the inclusion of streamlining effects in the parameterization of the mean and maximum wind-induced force. In Fig. 11(a) and (b) we show the Vogel exponent E and the pre-multiplier β parameter of the force to wind speed dependency, using a function $y = \beta x^{E+2}$, for the case of the mean and maximum force over 1-min periods. We see that as the wind speed interval increases from 0–6 to 0–13 m s^{-1} the Vogel exponent changes between −0.22 and −0.35. This shows that the streamlining effect get stronger as the wind speed is increasing. This trend is visible both in the mean and the maximum force. Furthermore, the decrease of the Vogel exponent is connected with an increase in the β parameter. As discussed in the work of Bekkers et al. (2022) the pre-multiplier β can have a physical interpretation when the drag coefficient and the frontal area of the tree are considered as wind speed dependent when the mean wind speed was greater than 5 m s^{-1}. We find that the ratio in the β values of the maximum and mean wind force is equal to 1.2 in the wind speed ranges from 0–6 to 0–13 m s^{-1} as seen in Fig. 11 (c).

Table 2
Values of the parameters β_c that E_c that can be used to estimate the maximum to mean force ratio using either the Method 1 or 2 and based on the equation and the $F_{max}/|\mathbf{F}| = \beta_c \cdot x^{E_c}$. The values of the parameters β_c that E_c have been estimated over different time periods ranging from 1 to 60 min.

Time period [min]	Summer tree				Winter tree			
	Method 1		Method 2		Method 1		Method 2	
	β_c	E_c	β_c	E_c	β_c	E_c	β_c	E_c
1	1.24	0.00	1.00	0.02	1.37	0.00	1.15	0.00
10	1.59	0.03	0.98	0.11	1.85	0.04	1.58	0.00
30	1.95	0.09	1.05	0.12	1.89	0.00	1.42	0.00
60	2.66	0.21	1.19	0.09	2.03	0.00	1.15	0.00

The results presented in Fig. 11 can be used to generate empirical functions that relate the mean to maximum force in the case of an open-grown oak tree. For this purpose, we consider that the ratio between the F_{max} and $|\mathbf{F}|$ is equal to $\beta_{max} \cdot x^{E_{max}+2} / \left(\beta_{mean} \cdot x^{E_{mean}+2}\right) = \beta_c \cdot x^{E_c}$. In Table 2 we present the values of the parameters β_c and E_c, which can be used to estimate the maximum force exerted on an open-grown tree, when the mean force is known. The values are calculated using the maximum force values from both the Method 1 and 2 from Fig. 10 and the mean 1-min values are used, since as we show in Fig. 8 the values β_{mean} and E_{mean} are independent of the time scale.

The tree studied is an open-grown tree that has grown in a rural environment, while being subject to strong wind conditions with consistent characteristics (i.e. direction). This is not necessarily the case for a typical urban tree, where the changes in the surroundings (e.g. construction activities, development of urban planning) can have an impact on the wind characteristics, or for forest trees. All trees acclimate to their local wind climate (Telewski, 1995) and, therefore, open-grown trees in rural areas will have to acclimate to more persistent mean winds and generally stronger maximum winds than urban

or forest trees in the same wind climate area. Thus, we cannot be sure about the universal description of the wind-interaction of an oak tree with foliage using a Vogel exponent equal to 1.65. However, as we show in Appendix C the assumption of a Vogel exponent equal to either −1 ($F \propto U$) or 0 ($F \propto U^2$) would lead to an under (or over) estimation of the wind load. Therefore, as highlighted by Cullen (2005), an accurate value of the Vogel exponent is necessary in order to realistically assess both the wind force on trees and the effect of trees on the surrounding wind field. This way an improved parameterization of trees in numerical simulations can be achieved which will benefit the study of the wind flow in urban environments (Hefny Salim et al., 2015).

The work presented in this paper is important for our understanding of the wind loads on solitary trees in urban environments and anywhere with potential risks to humans or human infrastructure. Such an understanding is useful for those concerned with urban tree safety (Ciftci et al., 2014) and the risk of tree fall on transport systems (e.g Gardiner et al., 2024). The methodology presented here can be also applied in studies of other trees in different circumstances to provide an indication of the likely mean and maximum wind loading on individual trees as a function of wind speed. The paper also provides a template for the testing of the wind loading on deciduous forest trees in summer and winter, an area of study that has been received surprisingly little attention (Jackson et al., 2019), which is important in providing a measure of the different levels of risk of damage at different times of the year. Already we are seeing in Europe an increasing level of wind damage in the summer months due to thunderstorms (e.g. Tadeusz Chmielewski and Bobra, 2020) when broadleaf trees are in-leaf. This is also predicted to be an increasing problem from remnant tropical hurricanes in western and northern Europe due to the changing climate (Haarsma et al., 2013) leading to stronger extreme winds in the August to October period when deciduous trees will be in-leaf.

5. Conclusions

We present field observations of the two-dimensional wind force exerted on an open grown oak tree. The main findings from this study can be summarized in the following points:

- We demonstrate that the two-dimensional mean and maximum wind force on a tree can be accurately estimated using two strain gauges installed on the stem of the tree.
- The tree's dynamic response behaves differently in the longitudinal axis which is aligned to the mean wind direction, compared to transverse axis. This observation is associated in general with a more evident eigen-frequency peak in the transverse, which is more pronounced in the winter than in the summer.
- The tree's two-dimensional response is highly correlated to the fluctuation of the horizontal wind vector at time scales greater than one minute.
- The two components of the horizontal mean force that is exerted on the tree can be well described using one Vogel exponent to describe the wind-induced reconfiguration of the crown. The value of the Vogel exponent depends on the crown state (i.e. with our without leaves).
- Two commonly used methods for calculating the maximum force were compared. The comparison showed significant and wind-speed dependent differences, which need to be taken into considered when evaluating and merging results from different sources.
- We show that the mean and maximum force can be described by the same wind speed parameterization dependency, when examining 1-min average data. This applied for both the winter and the summer tree and regardless the mean wind speed range. This points that the wind acclimated growth of trees results in a minimization of the mean and maximum loads in the same way.
- When focusing on the maximum wind force over a 10-min period, a typical time scale in wind engineering, then we find that in the wind speed range between 4–11 m s^{-1} the maximum force was 49%–66% and 52%–79% larger than the mean, during the summer and winter, respectively.

In summary, we have described a methodology that can be widely used for measuring maximum and mean wind loads on trees in urban and forest environments and in and out of leaf. These results will help in accurately quantifying the risk of wind damage to urban trees in particular.

CRediT authorship contribution statement

Nikolas Angelou: Writing – review & editing, Writing – original draft, Visualization, Validation, Software, Methodology, Investigation, Formal analysis, Data curation, Conceptualization. **Barry Gardiner:** Writing – review & editing, Methodology, Investigation. **Ebba Dellwik:** Writing – review & editing, Supervision, Resources, Project administration, Methodology, Investigation, Funding acquisition, Conceptualization.

Declaration of competing interest

The authors declare the following financial interests/personal relationships which may be considered as potential competing interests: Nikolas Angelou reports financial support was provided by Independent Research Fund Denmark. If there are other authors, they declare that they have no known competing financial interests or personal relationships that could have appeared to influence the work reported in this paper.

Acknowledgements

The contribution of the Lars Christensen, Søren William Lund and Michael Rasmussen research technicians in the *Measurements and Methods* section at DTU *Wind Energy and Systems* regarding the experiment setup, strain gauge calibration and measurement of the strain gauge positions is acknowledged. Barry Gardiner received financial supported from the Bundesministerium für Bildung und Forschung, project ClimXtreme (grant no. 01LP2324L). We further thank the Independent Research Fund Denmark, for financial support via The Single Tree Experiment, Grant no. DFF – 6111-00121.

Appendix A. Local wind climate

At a distance of approximately 700 m to the north-northwest direction from the location of the tree, a 120-m tall meteorological mast is located. The mast has been instrumented for the past 50 years with *in-situ* sensors (cup anemometers and wind vanes), providing measurements of the wind speed and direction, and other meteorological parameters like rain, solar radiation and temperature. Based on the measurements acquired at 76 m over the past 25 years, the wind climatology of the area is described by wind that originates predominately from the sector West-southwest to West-northwest (Fig. 12). According to the histogram of the horizontal wind speed of the direction sector 180°–360°, the wind conditions are characterized by an average of 7.2 ± 3.5 m s^{-1} and their spread can be described by a Weibull distribution with $a = 8.03$ and $k = 2.3$. We choose the 76 m, because it is the lowest height where flow distortion due to the surrounding surface heterogeneity introduced by the presence of the buildings and trees is not expected.

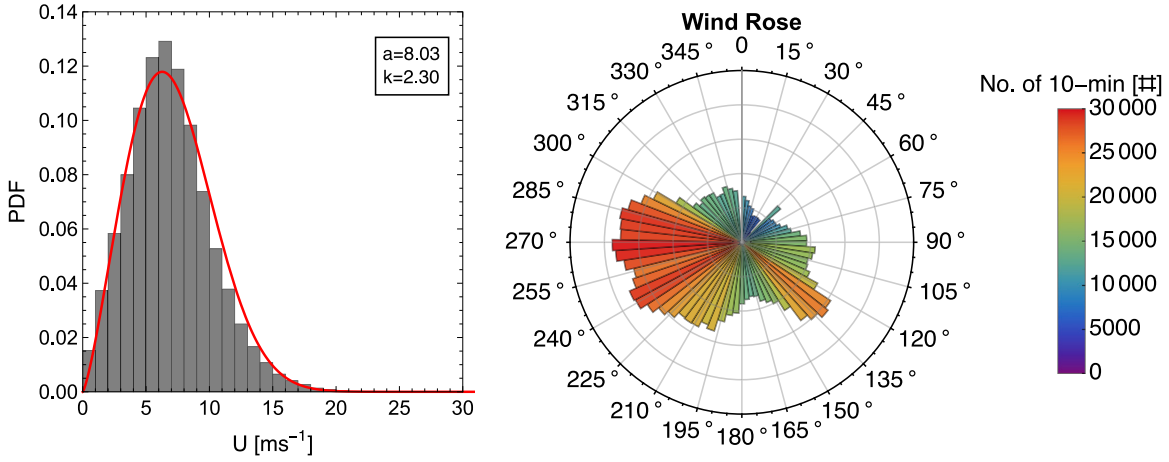

Fig. 12. Histogram of the 10-min mean wind speed and the corresponding wind rose measured at a height of 76 m at a distance 700 m from the tree between the years 1995 and 2023. The red curve in the histogram of the mean wind speed corresponds to a the probability density function of a Weibull distribution with parameters $a = 8.03$ and $k = 2.30$.

Appendix B. Strain gauge calibration

Each caliper transducer was instrumented with two strain gauges. The strain gauges were installed in a half-bridge configuration, where one gauge measured the deformation at the apex of the caliper transducer and the other gauge was used as passive to measure the strain induced by temperature (see Fig. 13). It has to be noted that this compensation does not take into account the temperature signal (s_t in Eq. (10)), which is induced by fixing the two arms of the caliper transducer on the tree and its magnitude is dependent on the diurnal and seasonal changes in the tree size. This was the reason of adding a temperature dependent strain contribution in Eq. (10).

The parameters in Eq. (6) describe the sensitivity of the two strain gauges. In order to quantify those parameters we performed two pulling tests, one for each tree state (summer and winter), by applying a static load from two different directions. The load was applied by adjusting the tension of a steel wire cable that was fixed between the tree and a vehicle (see Fig. 14).

Fig. 15 presents the setup of the static loading pulling tests used for the calibration of the two strain gauges, along with the corresponding loads presented in a two dimensional coordinate system. The two directions (#1 and #2) were used to calibrate the strain gauges by computing c_i using Eq. (2). The static load #1 was approximately aligned to the centre of the wind direction sector examined in this study. In general, the calibration showed that the strain gauge had a linear response to the externally applied load, which was measured with a S-type load cell (HBM, USA). In order to assess the accuracy of the calibration we applied a load from an additional, randomly selected direction (#3) and compared the applied load with the reconstructed one (see the results presented in Fig. 3).

We use a non-linear model fit to solve Eq. (3) based on the data acquired during the pulling tests. The results of the calibration are presented in Table 3.

Appendix C. Two-dimensional force estimation for different Vogel exponents

Fig. 16 presents the 1-min. mean longitudinal and transverse force that was exerted on the oak tree during the summer period. For the estimation of the force, instead of applying the method described in Angelou et al. (2019) we use two fixed values of the Vogel exponent E, in order to investigate the sensitivity of the results presented in Fig. 8

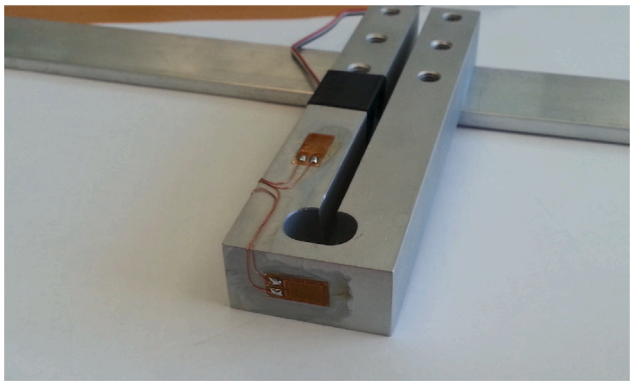

Fig. 13. Photograph of the active and passive strain gauges which were glued on the caliper transducer.

Table 3
Two-dimensional calibration parameters of the two strain gauges (S1 and S2) derived during two pulling static load test that were performed in the summer (2017-07-06) and the winter (2017-11-16). The c_i corresponds to the conversion factor between the bending moment exerted on the tree and the voltage measurement of the strain gauge, while the ϕ_i corresponds to the direction relative to the centre of the stem's cross section where the strain gauges were installed.

Date	Strain gauge	c_i [10^{-3} V N^{-1} m^{-1}]	ϕ_i [degrees]
2017-07-06	S1	0.063	170
2017-07-06	S2	0.045	87
2017-11-16	S1	0.072	170
2017-11-16	S2	0.035	87

to the values of E. The values correspond to the cases of considering a tree as: (i) a streamlined body ($E = -1$) and (ii) a bluff body ($E = 0$). In the case of $E = -1$ (Fig. 16 top row) we observe that this leads to a non-linear relationship between the longitudinal components of the force F_x and the wind $|\boldsymbol{U}|U_x$ vectors. This is a result of an erroneous estimation of the zero drift offset s_0 in Eq. (3). On the contrary, when the tree is treated as bluff body and thus $E = 0$, we have a linear relationship between the longitudinal F_x and the transverse F_y components and the corresponding components $|\boldsymbol{U}|U_x$ and $|\boldsymbol{U}|U_y$ of the wind. However the root mean square error ε for both components is higher than the corresponding results presented in Fig. 9.

Fig. 14. Photograph of a pulling test based on a static load used to calibrate the strain gauges installed at the base of the stem of the tree. In the photograph one can see the track used as an anchor, the steel wire used to apply a load on the tree, the oak tree and the meteorological mast used to study the wind conditions at the lee-side of the tree. At the time of this calibration, only one sonic anemometer was installed on the mast at 4 m above the ground.

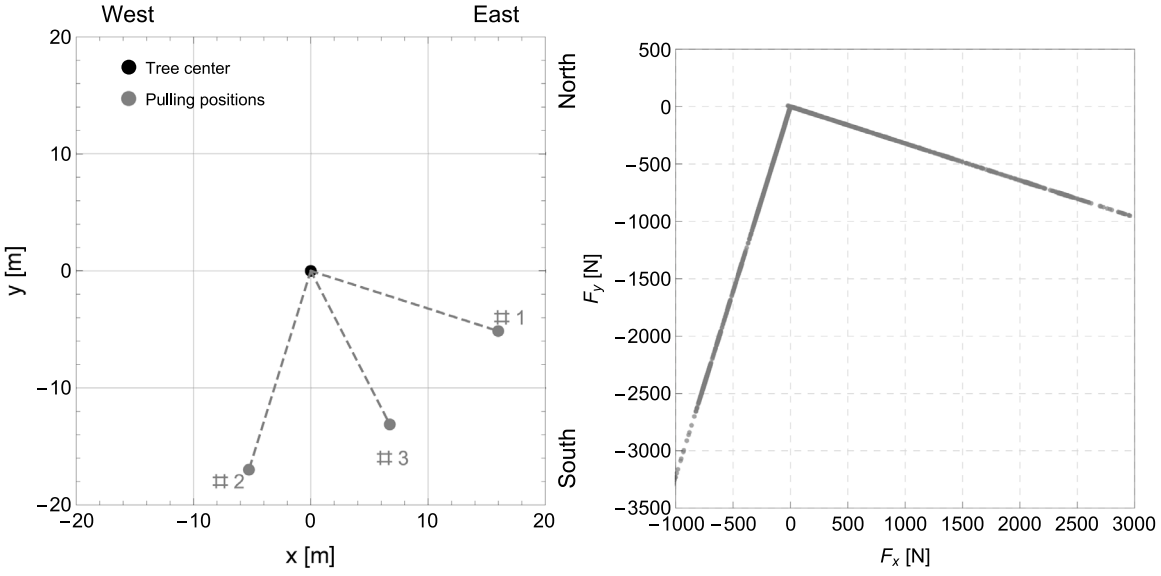

Fig. 15. Setup of the static loading pulling tests used for the calibration of the two strain gauges, along with the corresponding loads presented in a two dimensional coordinate system. The pulling points #1 and #2 where used for the calibration of the strain gauges. The pulling point #3 was used to assess the accuracy of the calibration.

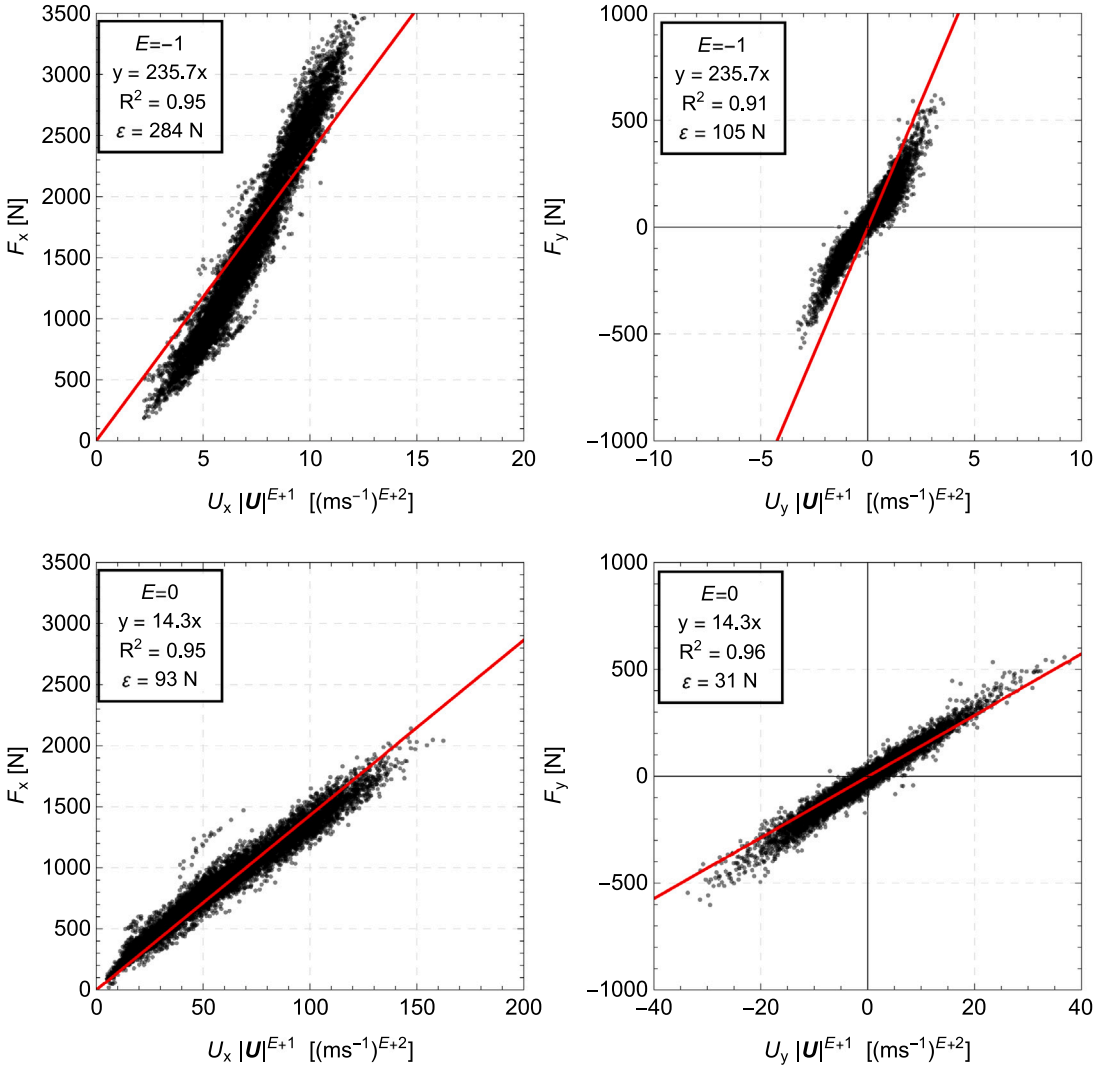

Fig. 16. Mean longitudinal (left column) and transverse (right column) force exerted on the oak tree during the summer period. The data used correspond to 1-min values, where E is equal to −1 (top row) and 0 (bottom column).

Data availability

Data will be made available on request.

References

Angelou, N., Dellwik, E., Mann, J., 2019. Wind load estimation on an open-grown European oak tree. For.: Int. J. For. Res. 92 (4), 381–392. http://dx.doi.org/10.1093/forestry/cpz026.

Angelou, N., Mann, J., Dellwik, E., 2021. Scanning Doppler lidar measurements of drag force on a solitary tree. J. Fluid Mech. 917, A30. http://dx.doi.org/10.1017/jfm.2021.275.

Barbacci, A., Diener, J., Hémon, P., Adam, B., Donès, N., Reveret, L., Moulia, B., 2014. A robust videogrametric method for the velocimetry of wind-induced motion in trees. Agric. For. Meteorol. 184, 220–229. http://dx.doi.org/10.1016/j.agrformet.2013.10.003.

Bekkers, C.C.A., Angelou, N., Dellwik, E., 2022. Drag coefficient and frontal area of a solitary mature tree. J. Wind Eng. Ind. Aerodyn. 220, 104854. http://dx.doi.org/10.1016/j.jweia.2021.104854.

Blackburn, G.R.A., 1997. The Growth and Mechanical Response of Trees to Wind Loading (Ph.D. thesis). University of Manchester, Available at https://isni.org/isni/0000000426817027.

Cao, J., Tamura, Y., Yoshida, A., 2012. Wind tunnel study on aerodynamic characteristics of shrubby specimens of three tree species. Urban For. Urban Green. 11 (4), 465–476. http://dx.doi.org/10.1016/j.ufug.2012.05.003.

Ciftci, C., Arwade, S.R., Kane, B., Brena, S.F., 2014. Analysis of the probability of failure for open-grown trees during wind storms. Probab. Eng. Mech. 37, 41–50. http://dx.doi.org/10.1016/j.probengmech.2014.04.002.

Cullen, S., 2005. Trees and wind: A practical consideration of the drag equation velocity exponent for urban tree risk management. Arboric. Urban For. 31 (3), 101–113. http://dx.doi.org/10.48044/jauf.2005.013.

Dellwik, E., van der Laan, M.P., Angelou, N., Mann, J., Sogachev, A., 2019. Observed and modeled near-wake flow behind a solitary tree. Agric. For. Meteorol. 265, 78–87. http://dx.doi.org/10.1016/j.agrformet.2018.10.015.

Gardiner, B.A., 1994. Wind and wind forces in a plantation spruce forest. Bound.-layer Meteorol. 67 (1–2), 161–186. http://dx.doi.org/10.1007/BF00705512.

Gardiner, B., Achim, A., Nicoll, B., Ruel, J.-C., 2019. Understanding the interactions between wind and trees: an introduction to the IUFRO 8th Wind and Trees Conference (2017). For.: Int. J. For. Res. 92 (4), 375–380. http://dx.doi.org/10.1093/forestry/cpz044.

Gardiner, B., Berry, P., Moulia, B., 2016. Review: Wind impacts on plant growth, mechanics and damage. Plant Sci. 245, 94–118. http://dx.doi.org/10.1016/j.plantsci.2016.01.006.

Gardiner, B., Blennow, K., Carnus, J., Fleischner, P., Ingemarson, F., Landmann, G., Lindner, M., Marzano, M., Nicoll, B., Orazio, C., Peyron, J., Reviron, M., Schelhaas, M., Schuck, A., Spielmann, M., Usbeck, T., 2010. Destructive storms in European Forests: Past and Forthcoming Impacts, Final report to European Commission - DG Environment. European Forest Institute, p. 138. http://dx.doi.org/10.13140/RG.2.1.1420.4006.

Gardiner, B., Lorenz, R., Hanewinkel, M., Schmitz, B., Bott, F., Szymczak, S., Frick, A., Ulbrich, U., 2024. Predicting the risk of tree fall onto railway lines. Forest Ecol. Manag. 553, http://dx.doi.org/10.1016/j.foreco.2023.121614.

Gardiner, B.A., Stacey, G.R., Belcher, R.E., Wood, C.J., 1997. Field and wind tunnel assessments of the implications of respacing and thinning for tree stability. Forestry 70 (3), 233–252. http://dx.doi.org/10.1093/forestry/70.3.233.

Gillies, J.A., 2002. Drag Coefficient and Plant Form Response to Wind Speed in Three Plant Species : Burning Bush (Euonymus alatus), Colorado Blue Spruce (Picea pungens glauca), and Fountain Grass (Pennisetum setaceum), Vol. 107, pp. 1–15 http://dx.doi.org/10.1029/2001JD001259.

Gosselin, F.P., 2019. Mechanics of a plant in fluid flow. J. Exp. Bot. 70 (14), 3533–3548. http://dx.doi.org/10.1093/jxb/erz288.

Haarsma, R.J., Hazeleger, W., Severijns, C., de Vries, H., Sterl, A., Bintanja, R., van Oldenborgh, G.J., van den Brink, H.W., 2013. More hurricanes to hit western Europe due to global warming. Geophys. Res. Lett. 40, 1783–1788. http://dx.doi.org/10.1002/grl.50360.

Hale, S.E., Gardiner, B.A., Wellpott, A., Nicoll, B.C., Achim, A., 2012. Wind loading of trees: Influence of tree size and competition. Eur. J. For. Res. 131 (1), 203–217. http://dx.doi.org/10.1007/s10342-010-0448-2.

Hao, Y., Kopp, G.A., Wu, C.-H., Gillmeier, S., 2020. A wind tunnel study of the aerodynamic characteristics of a scaled, aeroelastic, model tree. J. Wind Eng. Ind. Aerodyn. 197, 104088. http://dx.doi.org/10.1016/j.jweia.2019.104088.

Hassinen, A., Lemettinen, M., Peltola, H., Kellomäki, S., Gardiner, B., 1998. A prism-based system for monitoring the swaying of trees under wind loading. Agric. For. Meteorol. 90, 187–194. http://dx.doi.org/10.1016/S0168-1923(98)00052-5.

Hefny Salim, M., Heinke Schlünzen, K., Grawe, D., 2015. Including trees in the numerical simulations of the wind flow in urban areas: Should we care? J. Wind Eng. Ind. Aerodyn. 144, 84–95. http://dx.doi.org/10.1016/j.jweia.2015.05.004.

Hoag, D., Fridley, R., Hutchinson, J., 1971. Experimental measurement of internal and external damping properties of tree limbs. Trans. ASAE 14 (1), 20–0024. http://dx.doi.org/10.13031/2013.38215.

Högström, U., 1988. Non-dimensional wind and temperature profiles in the atmospheric surface layer: A re-evaluation. Bound.-Layer Meteorol. 42 (1), 55–78. http://dx.doi.org/10.1007/BF00119875.

Ishikawa, H., Amano, S., Yakushiji, K., 2007. Flow around a living tree. Jsme Int. J. Ser. B: Fluids Therm. Eng. 49 (4), 1064–1069. http://dx.doi.org/10.1299/jsmeb.49.1064.

Jackson, T.D., Sethi, S., Dellwik, E., Angelou, N., Bunce, A., van Emmerik, T., Duperat, M., Ruel, J.-C., Wellpott, A., Van Bloem, S., Achim, A., Kane, B., Ciruzzi, D.M., Loheide II, S.P., James, K., Burcham, D., Moore, J., Schindler, D., Kolbe, S., Wiegmann, K., Rudnicki, M., Lieffers, V.J., Selker, J., Gougherty, A.V., Newson, T., Koeser, A., Miesbauer, J., Samelson, R., Wagner, J., Ambrose, A.R., Detter, A., Rust, S., Coomes, D., Gardiner, B., 2021. The motion of trees in the wind: a data synthesis. Biogeosciences 18 (13), 4059–4072. http://dx.doi.org/10.5194/bg-18-4059-2021.

Jackson, T., Shenkin, A., Moore, J., Bunce, A., van Emmerik, T., Kane, B., Burcham, D., James, K., Selker, J., Calders, K., Origo, N., Disney, M., Burt, A., Wilkes, P., Raumonen, P., Gonzalez de Tanago Menaca, J., Lau, A., Herold, M., Goodman, R.C., Fourcaud, T., Malhi, Y., 2019. An architectural understanding of natural sway frequencies in trees. J. R. Soc. Interface 16, 20190116. http://dx.doi.org/10.1098/rsif.2019.0116.

James, K.R., Dahle, G.A., Grabosky, J., Kane, B., Detter, A., 2014. Tree biomechanics literature review: Dynamics. Arboric. Urban For. 40 (1), 1–15. http://dx.doi.org/10.13140/RG.2.1.1089.1765.

James, K., Haritos, N., Ades, P., 2006. Mechanical stability of trees under dynamic loads. Am. J. Bot. 93 (10), 1522–1530, URL www.jstor.org/stable/4123135.

Kaimal, J.C., Wyngaard, J.C., Izumi, Y., Coté, O.R., 1972. Spectral characteristics of surface-layer turbulence. Q. J. R. Meteorol. Soc. 98, 563–589. http://dx.doi.org/10.1002/qj.49709841707.

Kamimura, K., Nanko, K., Matsumoto, A., Ueno, S., Gardiner, J., Gardiner, B., 2022. Tree dynamic response and survival in a category-5 tropical cyclone: The case of super typhoon Trami. Sci. Adv. 8, http://dx.doi.org/10.1126/sciadv.abm7891.

Kane, B., Pavlis, M., Harris, J.R., Seiler, J.R., 2008. Crown reconfiguration and trunk stress in deciduous trees. Can. J. Forest Res. 38 (6), 1275–1289. http://dx.doi.org/10.1139/X07-225.

Kane, B., Smiley, E.T., 2006. Drag coefficients and crown area estimation of red maple. Can. J. Forest Res. 36 (8), 1951–1958. http://dx.doi.org/10.1139/x06-086.

Kitagawa, K., Iwama, S., Fukui, S., Sunaoka, Y., Yazawa, H., Usami, A., Naramoto, M., Uchida, T., Saito, S., Mizunaga, H., 2015. Effects of components of the leaf area distribution on drag relations for Cryptomeria japonica and Chamaecyparis obtusa. Eur. J. For. Res. 134, 403–414. http://dx.doi.org/10.1007/s10342-014-0859-6.

Kolbe, S., Pfenning, M., Schindler, D., 2024. Wind-induced torsional vibration in a ponderosa pine tree. Forest Ecol. Manag. 553, http://dx.doi.org/10.1016/j.foreco.2023.121638.

Kolbe, S., Rentschler, F., Frey, J., Seifert, T., Gardiner, B., Detter, A., Schindler, D., 2022. Assessment of effective wind loads on individual plantation-grown forest trees. Forests 13 (7), http://dx.doi.org/10.3390/f13071026.

Larsén, X.G., Larsen, S.E., Petersen, E.L., 2016. Full-scale spectrum of boundary-layer winds. Bound.-layer Meteorol. 159, 349–371. http://dx.doi.org/10.1007/s10546-016-0129-x.

Lieblein, J., 1976. Efficient Methods of Extreme-Value Methodology. Tech. Rep. NBSIR 74-602, National Bureau of Standards, http://dx.doi.org/10.6028/NBS.IR.74-602.

Lombardo, F.T., 2021. History of the peak three-second gust. J. Wind Eng. Ind. Aerodyn. 208, http://dx.doi.org/10.1016/j.jweia.2020.104447.

Manickathan, L., Defraeye, T., Allegrini, J., Derome, D., Carmeliet, J., 2018. Comparative study of flow field and drag coefficient of model and small natural trees in a wind tunnel. Urban For. Urban Green. 35, 230–239. http://dx.doi.org/10.1016/j.ufug.2018.09.011.

Mayhead, G.J., 1973. Some drag coefficients for british forest trees derived from wind tunnel studies. Agric. Meteorol. 12 (C), 123–130. http://dx.doi.org/10.1016/0002-1571(73)90013-7.

Moore, J.R., Gardiner, B.A., Blackburn, G.R., Brickman, A., Maguire, D.A., 2005. An inexpensive instrument to measure the dynamic response of standing trees to wind loading. Agricult. Forest. Meterol. 132 (1–2), 78–83. http://dx.doi.org/10.1016/j.agrformet.2005.07.007.

Peña, A., Dellwik, E., Mann, J., 2019. A method to assess the accuracy of sonic anemometer measurements. Atmos. Meas. Tech. 12 (1), 237–252. http://dx.doi.org/10.5194/amt-12-237-2019.

Roodbaraky, H., Baker, C., Dawson, A., Wright, C., 1994. Experimental observations of the aerodynamic characteristics of urban trees. J. Wind Eng. Ind. Aerodyn. 52, 171–184. http://dx.doi.org/10.1016/0167-6105(94)90046-9.

Rudnicki, M., Mitchell, S.J., Novak, M.D., 2004. Wind tunnel measurements of crown streamlining and drag relationships for three conifer species. Can. J. Forest Res. 34, 666–676. http://dx.doi.org/10.1139/x03-233.

Schindler, D., Bauhus, J., Mayer, H., 2012. Wind effects on trees. Eur. J. For. Res. 131 (1), 159–163. http://dx.doi.org/10.1007/s10342-011-0582-5.

Schindler, D., Schönborn, J., Fugmann, H., Mayer, H., 2013. Responses of an individual deciduous broadleaved tree to wind excitation. Agric. For. Meteorol. 177, 69–82. http://dx.doi.org/10.1016/j.agrformet.2013.04.001.

Schindler, D., Vogt, R., Fugmann, H., Rodriguez, M., Schönborn, J., Mayer, H., 2010. Vibration behavior of plantation-grown scots pine trees in response to wind excitation. Agric. For. Meteorol. 150 (7), 984–993. http://dx.doi.org/10.1016/j.agrformet.2010.03.003.

Spatz, H.C., Bruechert, F., 2000. Basic biomechanics of self-supporting plants: wind loads and gravitational loads on a Norway spruce tree. Forest Ecol. Manag. 135, 33–44. http://dx.doi.org/10.1016/S0378-1127(00)00296-6.

Syed, A.H., Mann, J., 2024. A model for low-frequency, anisotropic wind fluctuations and coherences in the marine atmosphere. Bound.-Layer Meteorol. 190 (1), http://dx.doi.org/10.1007/s10546-023-00850-w.

Tadeusz Chmielewski, J.S., Bobra, P., 2020. Derecho wind storm in Poland on 11–12 August 2017: results of the post-disaster investigation. Environ. Haz. 19, 508–528. http://dx.doi.org/10.1080/17477891.2020.1730154.

Tadrist, L., Saudreau, M., Hemon, P., Amandolese, X., Marquier, A., Leclercq, T., De Langre, E., 2018. Foliage motion under wind, from leaf flutter to branch buffeting. J. R. Soc. Interface 15 (142), http://dx.doi.org/10.1098/rsif.2018.0010.

Telewski, F.W., 1995. Wind-induced physiological and developmental responses in trees. In: Coutts, M.P., Grace, J. (Eds.), Wind and Trees. Cambridge University Press, pp. 237–263. http://dx.doi.org/10.1017/CBO9780511600425.015.

Vogel, S., 1984. Drag and flexiility in sessile organisms. Am. Zool. 24, 37–44. http://dx.doi.org/10.2307/3882750.

Vollsinger, S., Mitchell, S.J., Byrne, K.E., Novak, M.D., Rudnicki, M., 2005. Wind tunnel measurements of crown streamlining and drag relationships for several hardwood species. Can. J. Forest Res. 35, 1238–1249. http://dx.doi.org/10.1139/x05-051.

Wellpott, A., 2008. The Stability of Continuous Cover Forests (Ph.D. thesis). University of Edinburgh, Available at http://hdl.handle.net/1842/11534.

Whittaker, P., Wilson, C., Aberle, J., Rauch, H.P., Xavier, P., 2013. A drag force model to incorporate the reconfiguration of full-scale riparian trees under hydrodynamic loading. J. Hydraul. Res. 51, 569–580. http://dx.doi.org/10.1080/00221686.2013.822936.

Wyngaard, J.C., 2010. Turbulence in the Atmosphere. Cambridge University Press, Cambridge, ISBN: 9780511840524, http://dx.doi.org/10.1017/CBO9780511840524.